# Mössbauer study and molecular orbital calculations on the organo-iron (I, II) electron reservoir sandwiches CpFen+ ($\eta$6-C6(CH3)6) (n = 0,1) and related CpFe (cyclohexadienyl) complexes

J.P. Mariot, P. Michaud, S. Lauer, Dominique Astruc, A.X. Trautwein, F. Varret

Classification
*Physics Abstracts*
76.80 — 31.20P — 35.20

# Mössbauer study and molecular orbital calculations on the organo-iron (I, II) electron reservoir sandwiches $CpFe^{n+}$ ($\eta^6$-$C_6(CH_3)_6$) ($n$ = 0,1) and related CpFe (cyclohexadienyl) complexes

J. P. Mariot, P. Michaud (+), S. Lauer (++), D. Astruc (+), A. X. Trautwein (++) and F. Varret

Laboratoire de Spectrométrie Mössbauer (*), Faculté des Sciences, 72017 Le Mans Cedex, France

(*Reçu le 10 mars 1983, révisé le 21 juillet, accepté le 29 août 1983*)

**Résumé.** — Le sandwich paramagnétique réservoir d'électrons $\eta^5$-$C_5H_5Fe$(I) $\eta^6$-$C_6(CH_3)_6$ ainsi que sa forme diamagnétique monocationique oxydée et les complexes $\eta^5$-$C_5H_5Fe$ (cyclohexadienyl) correspondants ont été étudiés par spectrométrie Mössbauer sur des poudres et des monocristaux. Les spectres sous champ magnétique intense ont été enregistrés sur des poudres. A partir des données de rayons X, on a fait des calculs d'orbitales moléculaires I.E.H.T. qui ont donné des résultats en bon accord avec les données expérimentales à température ambiante et à 4,2 K. Les calculs d'OM montrent que la relaxation des orbitales moléculaires associée à la réduction électronique de II à I est négligeable ce qui permet de considérer un complexe de fer(I) comme la superposition d'un complexe de fer(II) et d'un électron. Cet électron occupe l'orbitale $e_1^*$ doublement dégénérée et a un très fort caractère métallique (83 %).

**Abstract.** — The paramagnetic Fe(I) electron reservoir sandwich $\eta^5$-$C_5H_5Fe$(I) $\eta^6$-$C_6(Me)_6$, its oxidized monocationic diamagnetic form and related diamagnetic $\eta^5$-$C_5H_5Fe$ (cyclohexadienyl) complexes have been studied by Mössbauer spectroscopy on powders and aligned crystals. Spectra under high magnetic field were recorded for powders. On the basis of X-ray data I.E.H.T. MO calculations were performed and gave results in good agreement with experimental data at room temperature and liquid helium temperature. The relaxation of molecular orbitals associated to the electronic reduction from II to I was found to be negligible, which enables to consider a Fe(I) complex as a superposition of a Fe(II) complex and one electron. This electron is occupying the doubly degenerate $e_1^*$ orbital and has a very strong metallic character (83 %).

## 1. Introduction.

Since the pioneering work of Collins [1] on ferrocene by Mössbauer spectroscopy and MO calculations, a large number of diamagnetic Fe(II) complexes have been studied [2, 3]. In particular the Mössbauer study of bridged ferrocenes [4] and the corresponding MO calculations gave consistent results. In these complexes the metal has a classical, $d^6$, Fe(II), 18 electrons configuration. According to Green's rule [5], this number 18 is found by adding the number of valence electrons of iron (8) and the number ($n$) of carbons coordinated to the iron ($\eta^n$ notation). For example ferrocene, $(\eta^5$-$C_5H_5)_2Fe$, is an 18 $e^-$ complex.

Recently we have reported a class of $d^7$, Fe(I), mixed 19 electrons (19 $e^-$) sandwiches, which are called Organometallic Electron Reservoirs [6-8]. These molecules have interesting chemical properties : high redox potential [9], redox catalytic activity [8], oxygen activation leading to $O_2^-$ production [10-12] and they are intermediate in organometallic mechanisms of electron or H atom transfer [13, 14]. Other $d^7$ 19 electrons sandwiches $(\eta^5$-$C_5H_5)_2Co$, $(\eta^5$-$C_5H_5)_2Ni^+$, $(\eta^6$-$C_6Me_6)_2Fe^+$, $(\eta_6$-$C_5H_5Br)Co$ (R = alkyl, phenyl, Me = methyl) have been studied through magnetism, EPR [15] and paramagnetic NMR [16] spectroscopy. Their molecular orbital diagram is now well established from the qualitative point of view.

We must emphasize here the importance of the quantitative knowledge of the MO functions which enables us to calculate any physical observable, for instance electronic (Electric Field Gradient (EFG) tensor, Isomer Shift (IS)) and magnetic (hyperfine field

(+) Laboratoire de Chimie des Organométalliques, Université de Rennes, 35042 Rennes Cedex, ERA CNRS 477.
(++) Institut für Physik, Medizinische Hochschule, D 2400 Lübeck 1, F. R. G.
(*) ERA CNRS 682.

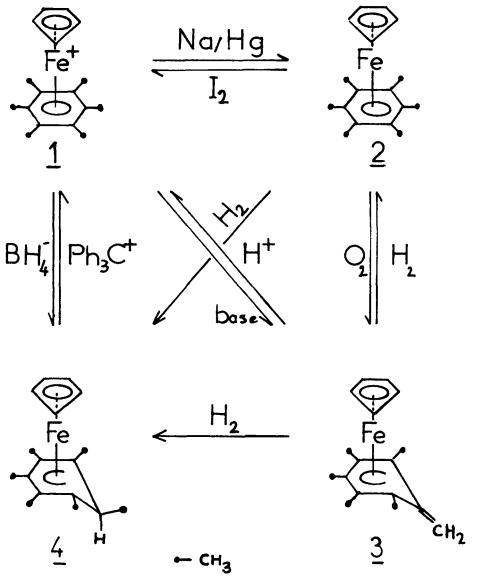


Fig. 1*a*. — The four compounds numbered from 1 to 4. The possible ways of synthesis are shown by arrows.

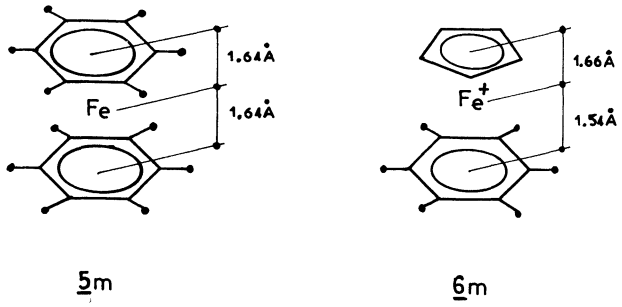


Fig. 1*b*. — Compounds 5m (20 $e^-$) and 6m (18 $e^-$).

tensor) properties. We focussed here on electronic properties. These calculations are the basis of the interpretation of the physical properties of the complexes.

Here we present the study of four compounds shown on figure 1. 1, 3 and 4 are $d^6$, Fe(II), 18 $e^-$ diamagnetic compounds and 2 is a $d^7$, Fe(I) 19 $e^-$ paramagnetic compound. Their respective colours are yellow (1), forestgreen (2), red (3) and orange (4). On the basis of X-ray structural data, semi-empirical MO calculations were performed and their results are compared here with measured Mössbauer hyperfine parameters, which partially date back to earlier publications [6, 17, 20]. In addition, other spectroscopic tools were used but their results are presented elsewhere [9, 18].

## 2. Synthesis and preparation of the Mössbauer samples.

2.1. For synthesis of the compounds, we refer to references 7, 12.

2.2 PREPARATION OF MÖSSBAUER SAMPLES. — All the Mössbauer samples were conditioned under nitrogen atmosphere in a plastic cell, sealed with epoxy glue. For powders this was done in a glove bag, for aligned crystals under a glove box. For 2, two aligned crystal samples were prepared considering the positions of the axes of the monoclinic structure : one with *c* parallel to the propagation direction of the $\gamma$-rays (labelled $\gamma_1$) and the other with *b* parallel to this direction (labelled $\gamma_2$).

## 3. MO calculations for 2, 3, and 4.

3.1 X-RAY DATA (Fig. 3). — Crystallographic data are available for 2, 3 and 4 [19, 20], MO calculations were made on « real » structures (letter r in table Ia) or « model » structures (letter m in table I*a*). Real

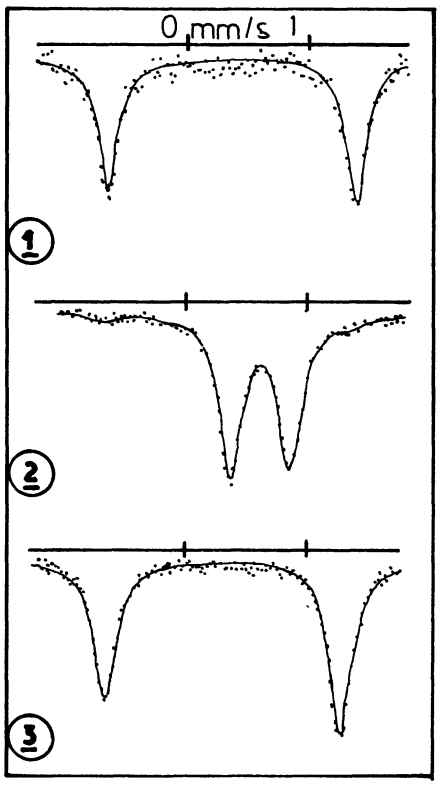


Fig. 2. — Spectra of 1, 2 and 3 at room temperature. The higher IS and smaller $\Delta E_Q$ must be noted for 2. A small texture was found for 2 and 3. 4 is very similar to 3.

structures are obtained from X-ray measurements. Model structures were also used

(i) for compounds of unknown X-ray data (5m shown in Fig. 1*b*),

(ii) in order to get the highest possible symmetry of the complexes : for 2m, 2m′ and 2m″ we took exact

Table Ia. — MO *results for* 2, 3, 4. *Ferrocene data have been added for reference.* 5m *is a* Fe(0) 20 $e^-$. 6m *is a* 18 $e^-$ *compound modelized from* 2r' (*see Fig.* 1b). *The absolute experimental error on* $\Delta E_Q$ *and IS is* ± 0.01 mm/s. *IS is relative to metallic iron at room temperature. Experimental data were recorded at room temperature.*

| | ferrocene | 3r | 4r | 2r | 2r' | 2m | 2m' | 2m'' | 5m | 6m |
|---|---|---|---|---|---|---|---|---|---|---|
| excess/18 $e^-$ | 0 | 0 | 0 | 1 | 1 | 1 | 1 | 1 | 2 | 0 |
| oxidation state | II | II | II | I | I | I | I | I | 0 | II |
| number of AO | 59 | 99 | 101 | 100 | 100 | 100 | 100 | 100 | 69 | 100 |
| number of $e^-$ | 58 | 98 | 100 | 99 | 99 | 99 | 99 | 99 | 68 | 99 |
| $q_{at}$ (Fe) in $e_0$ | 0.155 0 | 0.131 6 | 0.156 1 | 0.124 9 | 0.126 0 | 0.126 1 | 0.126 4 | 0.126 1 | 0.107 2 | 0.262 0 |
| $N_{4s}$ (Fe) | 0.200 4 | 0.188 5 | 0.192 9 | 0.185 8 | 0.202 9 | 0.172 5 | 0.218 9 | 0.218 9 | 0.144 0 | 0.182 1 |
| $N_{4p}$ (Fe) | 1 339 5 | 1.161 3 | 1.146 1 | 1.055 4 | 1.133 2 | 0.978 3 | 1.220 6 | 1.221 0 | 0.811 3 | 1.104 5 |
| $N_{3d}$ (Fe) | 6.484 9 | 6.649 9 | 6.620 9 | 6.829 2 | 6.786 5 | 6.870 5 | 6.763 0 | 6.760 8 | 7.043 0 | 6.500 9 |
| $\Delta E_Q$ in mm/s | 2.85 | 2.61 | 2.90 | 1.27 | 0.99 | 1.53 | 0.67 | 0.67 | − 1.05 | 2.59 |
| $\eta$ | 0 | 0.57 | 0.85 | 0.17 | 0.22 | 0 | 0 | 0 | 0 | 0.13 |
| $\theta$ = (Oz, OZ) in degrees | 0 | 9.5 | 10 | 4.5 | 6.2 | 0 | 0 | 0 | 0 | 2.5 |
| $\rho(0)$ in $a_0^{-3}$ | 15 067.56 | 15 066.91 | 15 066.82 | 15 065.64 | 15 065.90 | 15 065.44 | 15 066.26 | 15 066.26 | 15 064.73 | 15 067.22 |
| $\Delta E_{Q_{exp}}$ in mm/s | 2.40 | 1.89 | 1.96 | 0.5 | 0.5 | 0.5 | 0.5 | 0.5 | − 1.45 | 1.89 |
| $IS_{exp}$ in mm/s | 0.45 | 0.45 | 0.45 | 0.74 | 0.74 | 0.74 | 0.74 | 0.74 | 1.02 | 0.45 |
| $\eta_{exp}$ | ~ 0 | 0.40 | 0.57 | ~ 0 | ~ 0 | ~ 0 | ~ 0 | ~ 0 | ~ 0 | ~ 0 |

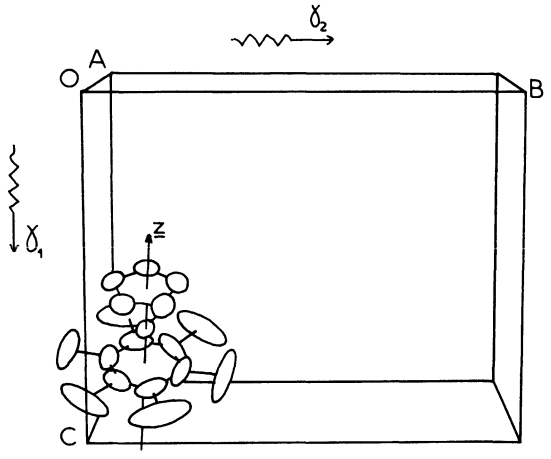


Fig. 3. — Perspective view of the molecule of 2 in the monoclinic structure. $a$ = 8.363 Å, $b$ = 14.710 Å, $c$ = 11.845 Å, $\beta$ = 93°.98. $z$ is the molecule axis and ($z$, $c$) = 30°, ($z$, $b$) = 86°.

$C_S$ symmetry with the cyclopentadienyl ($Cp = C_5H_5$) ring parallel to the arene ($C_6(CH_3)_6$) ring.

For 2 where a phase transition is found to occur [6, 19] at 190 K, only the high temperature structure has been determined : $P_{21/c}$ ; we kept the same intramolecular distances at low temperatures for MO calculations.

3.2 INTERMOLECULAR CONTRIBUTIONS. — In order to investigate the various contributions to the Electric Field Gradient tensor (EFG), we have prepared a sample by cosublimating 2 and 4 which have the same packing. This cosublimation was done in 1/1 ratio, which is reflected by the Mössbauer spectrum of figure 4 (same areas of subspectra). The observed

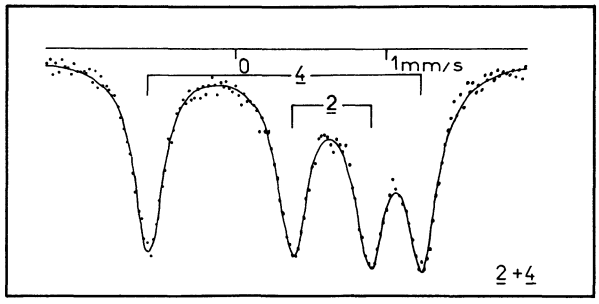


Fig. 4. — Experimental Mössbauer spectrum of 2 diluted in 4 recorded at room temperature. The relative areas of the subspectra agree well with the chemical preparation (1/1 ratio of 2 and 4).

quadrupole splittings $\Delta E_Q$ for $\underline{2}$ + $\underline{4}$ are the same as those obtained for $\underline{2}$ alone and $\underline{4}$ alone respectively. This result indicates that intermolecular contributions to the EFG can be neglected. Thus the MO results, which represent intramolecular contribution only, are significant.

3.3 APPROXIMATE MOLECULAR ORBITAL CALCULATIONS. — The MO calculations have been performed on the basis of the Iterative Extended Hückel Theory (I.E.H.T.) formalism [21] where we take only valence electrons into account. As the iron nucleus is surrounded by carbons (C) and hydrogens (H), we take atomic orbitals (AO) 2s, 2p for C and 1s for H ; for iron we take 4s, 4p and 3d AO. For instance, for $\underline{2}$ whose formula is $C_{17}H_{23}Fe$ we need $17\times4+23+9=100$ AO. Similarly the number of electrons is evaluated : 4 for C, 1 for H and 8 for iron which lead to $4\times17+23+8=99$ $e^-$. The number of MO is equal to the number of AO. The first 98 $e^-$ are occupying the 49 lowest MO (2 $e^-$ of opposite spin on each MO) and the 99th $e^-$ is shared equally into MO 50 and MO 51 for the high temperature structure.

The method is semi empirical in the sense that the diagonal matrix elements of the total Hamiltonian of the system are built using ionization potentials of the C, H and Fe atoms. Off-diagonal elements are calculated using the Cusachs approximation [21]. The convergence is made on the charge of the atoms in a self-consistent way. Once the MO $\phi_i$ are known, one can calculate any physical observable $\langle O \rangle$ :

$$\langle O \rangle = \sum_{i=1}^{occ} n_i \langle \phi_i | \hat{O} | \phi_i \rangle \qquad (1)$$

where the summation is made on the occupied MO and $n_i$ is the number of $e^-$ in MO $\phi_i$. The MO are taken as linear combinations of AO $\psi_\mu$

$$\phi_i = \sum_\mu C_{i\mu} \psi_\mu . \qquad (2)$$

Hence (1) becomes :

$$\langle O \rangle = \sum_{\mu\nu} P_{\mu\nu} \langle \psi_\mu | \hat{O} | \psi_\nu \rangle \qquad (3)$$

where $P_{\mu\nu}$ are the bond order matrix elements :

$$P_{\mu\nu} = \sum_{i=1}^{occ} n_i C_{\mu i} C_{\nu i} .$$

In Mössbauer spectroscopy, where we measure at a specific site $k$ within a molecular system, we may distinguish three kinds of $\langle \psi_\mu | \hat{O} | \psi_\nu \rangle$ contributing to $\langle O \rangle$ : (i) $\psi_\mu$ and $\psi_\nu$ belong to site $k$ (valence contribution) ; (ii) only $\psi_\mu$ belongs to site $k$ but $\psi_\nu$ to a ligand (overlap contribution) ; (iii) $\psi_\mu$ and $\psi_\nu$ both belong to ligands (ligand contribution).

Using the self consistently derived MO, we have evaluated the EFG tensor and the electronic charge density of the iron nucleus with the schemes described previously [22, 23]. However, since the calculation of the three centre contribution (ligand contribution) to the EFG is rather time consuming, we were using an approximation instead. The overlap charges between ligand atoms have been located as point charges midway between the ligand atoms and a point charge model has been used to calculate their contribution to the EFG. This procedure has been tested for ferrocene, where large overlap charges between the carbon ring atoms yield a considerably large three centre contribution to the EFG which is comparable in magnitude with the one centre contribution. Comparing this approximation with a numerical integration we found a difference of only about 5 % (0.2 mm/s).

The calculation of the electronic charge density ($\rho(0)$) was performed using the molecular wave functions and the iron core *ns* Hartree-Fock (HF) functions [24] which have been orthogonalized to the molecular orbital wave functions [23]. Differing from a former investigation [4] where HF functions have been used to represent also the ligand orbitals we have used here Slater Type Orbitals (STO) instead. This results in slightly shifted absolute charge density values as compared to the former investigation. However, this is of no importance since physical significance is attributed only to differences in $\rho(0)$ when comparing various compounds.

3.4 MO RESULTS. — They appear on table I*a*. Ferrocene is given as a reference. For the modelized structure of $\underline{2}$, C-C distances and C-H distances were taken as 1.42 Å and 1.05 Å respectively and various Cp-Fe and Fe-arene distances were choosen to evaluate the dependence of EFG with respect to the geometry of the molecule. (table I*b*), The two possibilities for Cs symmetry were tried ($\underline{2}$m', $\underline{2}$m") and lead to no significant difference. The compound $\underline{6}$m was derived from $\underline{2}$r' : the intermolecular distances remain the same, except for Fe-Cp distance (see table I*b*) but it has only 18 $e^-$ and thus a positive charge. The discussion of the results is done in section 5.4. A 20 $e^-$ compound

Table I*b*. — Fe-Cp *and* Fe-*arene distances* (in Å).

| | ferrocene | $\underline{3}$r | $\underline{4}$r | $\underline{2}$r | $\underline{2}$r' | $\underline{2}$m | $\underline{2}$m', $\underline{2}$m" | $\underline{5}$m | $\underline{6}$m |
|---|---|---|---|---|---|---|---|---|---|
| Fe-Cp | 1.64 | 1.66 | 1.66 | 1.78 | 1.76 | 1.78 | 1.66 | | 1.66 |
| Fe-arene | | 1.54 | 1.54 | 1.58 | 1.54 | 1.58 | 1.50 | 1.66 | 1.54 |

(5m) (see Fig. 1*b*) has been added for comparison, but corresponding results will be published elsewhere.

## 4. Mössbauer data.

### 4.1 Quadrupolar spectra (Figs. 2, 5).

4.1.1 *Diamagnetic compounds* 1, 3, 4. — They give hyperfine parameters similar to those of ferrocene.

4.1.2 *Paramagnetic compound* 2. — Powder and two samples of aligned crystals were studied (see Figs. 2, 5). The first aligned crystal ($\gamma_1$) was recorded at both room and liquid helium temperatures. The second one ($\gamma_2$) was only recorded at room temperature because of its low counting rate. The oxidized complex 3 was found as an additional contribution in most spectra.

The EFG tensor sign was found to be unambiguously positive at room temperature from line intensities. At low temperature, the line intensities are not different enough to remove the ambiguity on the sign of the EFG. However, when only the lower $e_1^*$ level (MO 50) is populated, a negative sign is expected, associated with a change of the principal axis ($Z$) of the EFG tensor (Table II*a*), which becomes perpendicular to the molecular axis ($z$). Then the measured line intensity ratios were used to determine the orientation of $Z$ (the EFG tensor is assumed positive axial at room temperature and negative axial at low temperature), with respect to the sample plane : the experimental results agree with MO expectations (Table II*b*). The little deviation at low temperature can be due to thickness effects neglected when fitting the experimental spectrum. These effects are much lower at room temperature because of the low value of the Debye temperature, about 130 K [25].

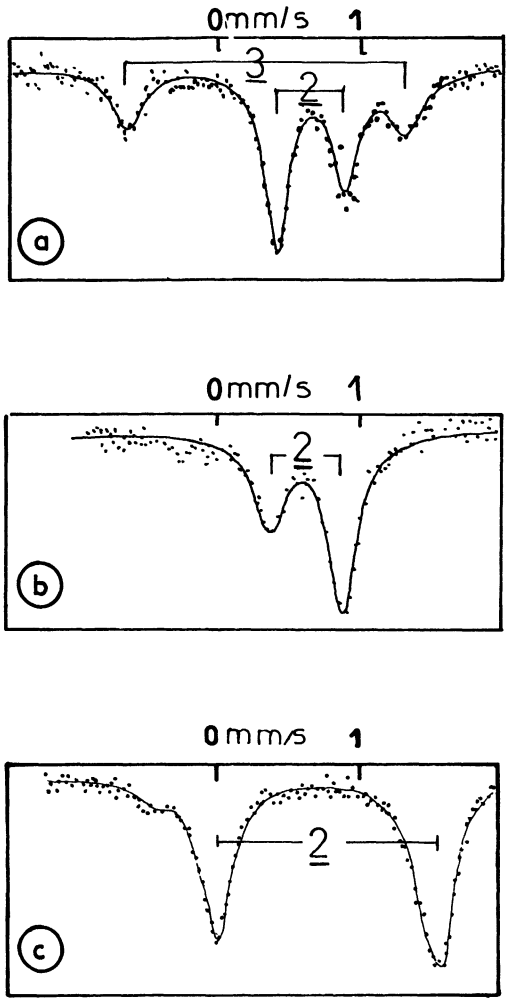


Fig. 5. — Spectra of aligned crystals of 2. The following parameters were fitted : $\Delta E_Q$, IS and line intensities $I_1$, $I_2$ ; (*a*) at 300 K, $I_1/I_2 = 1.91$ ($\gamma_2$); (*b*) at 300 K, $I_1/I_2 = 0.60$ ($\gamma_1$); (*c*) at 4.2 K, $I_1/I_2 = 0.84$ ($\gamma_1$).

4.2 Spectra under magnetic field. — The asymmetry parameter $\eta$ of the EFG tensor is defined by $\eta = \frac{V_{xx} - V_{yy}}{V_{zz}}$ where $V_{xx}$, $V_{yy}$ and $V_{zz}$ are the eigenvalues of the EFG tensor such as $|V_{zz}| > |V_{yy}| > |V_{xx}|$. $\Delta E_Q$ is proportional to $V_{zz}\left(1 + \frac{\eta^2}{3}\right)^{1/2}$. Only absolute value of $\Delta E_Q$ can be obtained from quadrupolar spectra. The determination of $\Delta E_Q$ sign and $\eta$ value requires high magnetic field (6 T) measurements.

The 6 T magnetic field parallel to the $\gamma$-rays was supplied by a superconducting magnet in which the Mössbauer source was held at the same temperature as the absorber. Thus the IS can be taken as temperature independent.

Table IIa. — *Cosines of* EFG *axes* ($X$, $Y$, $Z$) *with respect to molecule axes* ($x$, $y$, $z$) *at high* (*left*) *and low* (*right*) *temperature for* 2r. *Axes are labelled according to* $|V_{ZZ}| > |V_{YY}| > |V_{XX}|$.

| | $X$ | $Y$ | $Z$ |
|---|---|---|---|
| $x$ | − 0.475 2 | 0.878 8 | − 0.043 4 |
| $y$ | − 0.876 3 | − 0.472 2 | − 0.066 9 |
| $z$ | − 0.079 5 | 0.006 2 | 0.996 8 |

| | $X$ | $Y$ | $Z$ |
|---|---|---|---|
| $x$ | − 0.422 0 | 0.248 3 | 0.871 9 |
| $y$ | − 0.762 0 | 0.411 5 | − 0.489 4 |
| $z$ | 0.480 3 | 0.876 9 | − 0.071 2 |

Table IIb. — *Angle β between* EFG *axis and γ-rays for* 2 *; assumptions are explained in section* 4.1.2. *The letters a, b, c, refer to the spectra of figure* 5.

| | *a* | *b* | *c* |
|---|---|---|---|
| $\beta_{exp}$ | 30° | 117° | 90° |
| $\beta_{calc}$ | 30° | 104° | 86° |

4.2.1 *Diamagnetic samples* (Fig. 6). — As expected 1, 3 and 4 behave as diamagnets under the applied field and exhibit a positive sign for $\Delta E_Q$, like ferrocene [1]. In agreement with MO results, 3 and 4 have large $\eta$ (Table I*a*).

4.2.2 *Paramagnetic sample* (Fig. 7). — To discuss the behaviour of paramagnetic complex 2, we used a formalism previously described [26] : the applied field **H** creates a hyperfine field $\mathbf{H}_i$ according to the linear relation $\mathbf{H}_i = |A||g^{-1}||\chi|\mathbf{H} = |B|\mathbf{H}$ leading to the effective field $\mathbf{H}_e = \mathbf{H} + \mathbf{H}_i = |1 + B|\mathbf{H}$. The « effective field tensor » $|1 + B|$ obeys the point symmetry at the iron nucleus. The relevance of this model and the resulting magnetic data will be discussed elsewhere.

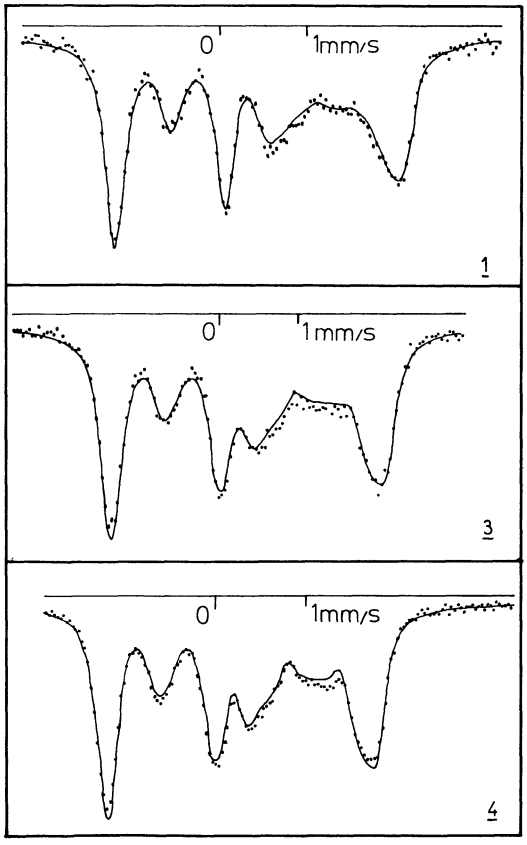


Fig. 6. — Diamagnetic compounds under 6 T. IS, $\Delta E_Q$ and $\eta$ were fitted. Computer fit is similar to that of Collins and Travis [33].

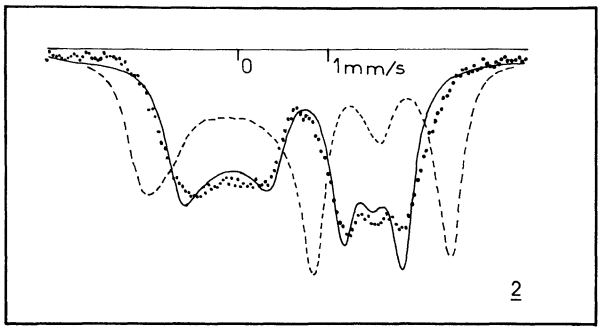


Fig. 7. — Paramagnetic compound 2 under 6 T at 4.2 K. IS, $\Delta E_Q$ and hyperfine field were fitted. The dashed line shows the spectrum for a zero hyperfine field (diamagnetic assumption). From the fit [34] we get $HB_x = -3.7$ T, $HB_y = -3.7$ T, $HB_z = -2.3$ T.

From figure 1 the paramagnetic behaviour of 2 and a negative sign for $\Delta E_Q$ can be concluded. In the fit we took an axial EFG tensor consistent with the aligned crystal experiments and MO results.

## 5. Discussion.

5.1 EFG TENSORS. — Comparing the calculated $\Delta E_Q^{calc}$ and experimental $\Delta E_Q^{exp}$ in table I*a*, we find for all systems a difference of 0.5 mm/s at least. However all the molecules have a very large contribution arising from the Fe 4p electrons (ranging from − 0.7 to − 1.4 mm/s) and therefore inaccuracies in the calculation of the 4p contribution will play an important rôle. One source of an inaccurate estimate of the 4p contribution may be the lack of a calculation of the Sternheimer correction $(1 - R_{4p})$ for the 4p electrons ; $R_{3d}$ has been used so for instead. $R_{3d}$ including the polarization of the valence electrons takes the value 0.12 [27-29] while in the MO calculations being performed in this work a modified value for $R_{3d}$, which excludes the polarization of the valence electrons has been used ($R_{3d} = 0.08$ [29]). However to overcome the problems associated with the use of $R_{4p}$ as being identical to $R_{3d}$ we calculated $R_{4p}$ according to the scheme outlined in [29]. As Fe 4p wave functions we used the 4p Slater Type Orbitals (STO) ($r^{n-1} e^{-\xi r}$ with $\xi = 1.4$) which were orthogonalized to the Fe Hartree-Fock wave functions taken from Clementi [24]. For configurations $3d^7 4s^0$, $3d^6 4s^1$, and $3d^6 4s^0$ we found a value which is pratically constant ($R_{4p} = -0.31$) and is nearly the same if the polarization of the valence electrons (4s, 3d) is excluded.

This large negative Sternheimer correction agrees with other calculations for external p functions in I [29], W and Cs [30]. Due to this modified Sternheimer correction, the 4p contribution to the EFG will be changed by about 40 % (+ 0.08 to − 0.31). If this 4p correction is done on the total EFG, we find a very good agreement between calculated and measured values. But, for systems with a large asymmetry parameter, the calculated $\eta$ increases by about 0.2 after the

correction and is no longer consistent with experimental values. This discrepancy might be due to less accurate X-ray structure determination for these molecules, as compared to the systems with a vanishing asymmetry parameter. In addition all the systems under investigation in this work have large bond order matrix elements $P_{4s,3d_{z^2}}$ (about $-0.20$) thus giving rise to a small, but non vanishing contribution to the EFG calculated from the iron 4s and 3d functions. Although the magnitude of this contribution is difficult to estimate, its sign behaves so as to improve the calculated $\eta$. Nevertheless only qualitative agreement is obtained for $\eta$ leading to large values for 3 and 4 which probably originate from both the uncoordinated carbon on the arene and the shift of the arene in the $xy$ plane. On the contrary a small $\eta$ has been measured on 1 ($\eta < 0.15$) which can be explained by the symmetry of the molecule where the arene is fully coordinated to iron.

Another alternative to decrease the calculated EFG is to compress the molecule along the 2 axis. For instance in comparing 2r and 2r', a 0.03 Å compression, which keeps in the error bar limit, decreases $\Delta E_Q$ by 0.28 mm/s ; the same order of magnitude was given for ferrocene [5] where a 0.02 Å compression decreases $\Delta E_Q$ by 0.17 mm/s. A drastic compression was made on 2m leading to 2m' where $\Delta E_Q =$ 0.67 mm/s, still 0.17 mm/s larger than the experimental 0.5 mm/s. Thus these geometrical changes are not sufficient for improving the agreement between calculated and experimental parameters.

5.2 ISOMER SHIFTS (IS). — The measured IS are related to the electronic density on the nucleus $\rho(0)$, through $IS = Cst + \frac{4}{5}\pi Ze^2\ \rho(0)\ R\ \delta R$ [31]. The nuclear factor can be directly determined so the IS calibration constant $\alpha = \dfrac{\Delta IS_{exp}}{\Delta\rho(0)_{calc}}$ is used. Experimental determinations on various systems give $\alpha$ near $-0.2\ a_0^3$ mm/s [23]. Several values can be derived from table I comparing :

(i) ferrocene − 2r $\quad \alpha = -0.15\ a_0^3$ mm/s
(ii) ferrocene − 2r' $\quad \alpha = -0.18\ a_0^3$ mm/s
(iii) 3r − 2r $\quad \alpha = -0.23\ a_0^3$ mm/s
(iiii) 4r − 2r $\quad \alpha = -0.25\ a_0^3$ mm/s
(iiiii) 2r' − 5m $\quad \alpha = -0.24\ a_0^3$ mm/s

5.3 IRON TOTAL CHARGE (see Table I). — It is worth considering the effect of electronic reduction. As expected for a decrease in the iron oxidation state from II to I, the total charge $q_{at}$(Fe) is decreased. However this decrease is far smaller than in the case of ionic compounds. Similarly the 3d orbital occupation number $N_{3d}$ increases because of the metallic contribution of the extra electron, but slightly.

5.4 METALLIC CHARACTER OF THE HIGHEST OCCUPIED MOLECULAR ORBITAL (HOMO) IN 2. — It can be derived from MO 50 and MO 51 expressions calculated for 2r' :

$$MO\ 50 = 0.003\ 1\ d_{xy} + 0.449\ 1\ d_{yz} + 0.023\ 4\ d_{z^2} - 0.802\ 8\ d_{xz} + 0.008\ d_{x^2-y^2} + \phi_{lig}$$

$$MO\ 51 = 0.019\ 6\ d_{xy} + 0.791\ 1\ d_{yz} + 0.005\ d_{z^2} + 0.442\ 6\ d_{xz} + 0.009\ 9\ d_{x^2y^2} + \phi'_{lig}\ .$$

It must be noted that MO 50 and MO 51 have mainly $d_{xz}$ and $d_{yz}$ character originating from the $e_1$ iron atomic orbitals. The metallic 3d character of the HOMO is respectively 85 % for MO 50 and 82 % for MO 51. However the difference between the metallic character of MO 50 and MO 51 is not realistic because it originates from the energy difference between MO 50 and MO 51 which is over-estimated. The average value 83.5 % is more significant ; MO 50 and MO 51 should be modelized [32] as :

$$\phi_{50} = 0.91\ d_{xz} + \phi_{lig}$$

$$\phi_{51} = 0.91\ d_{yz} + \phi'_{lig}\ .$$

The calculated prominent cyclopentadienyl character of $\phi_{lig}$ (or $\phi'_{lig}$) also observed by NMR [6] explains the increase of Cp-Fe distance from 3 (or 4) to 2.

5.5 A MODEL FOR THE EFG TENSOR OF 2. — Of particular interest is the relaxation of molecular orbitals associated with the electronic reduction (from II to I). The contribution of the first 49 MO has been calculated in 2r' : $\Delta E_Q^{(49)} = 2.59$ mm/s, $\eta^{(49)} = 0.06$ ; the ligand contribution of MO 50, 51 to $\Delta E_Q$ was small : 0.10 mm/s (the remainder was due to $d_{xz}$ and $d_{yz}$). Calculations for a comparable 49 MO model, 6m gave $\Delta E_Q = 2.59$ mm/s, $\eta = 0.12$, indicating that relaxation is negligible. Then it is possible to modelize a Fe(I) complex by adding the contributions of the corresponding Fe(II) complex and of the metallic orbitals $d_{xz}$, $d_{yz}$ with a covalency factor 0.83. The reliability of this model mainly depends upon the relaxation results for :

(i) the covalency factor is rather well calculated
(ii) we take for the EFG tensor $V_{pq}^{49}$ the experimental value.

The metallic orbitals $d_{xz}$, $d_{yz}$ are responsible for the temperature dependence of Fe(I) paramagnetic complexes EFG tensor components :

$$V_{pq}(T) = V_{pq}^{(49)} + V_{pq}^{(3d)}(T)$$

where

$$V_{pq}^{3d}(T) = [V_{pq}^{(1)} + V_{pq}^{(2)} \exp(-\Delta/kT)]/[1 + \exp(-\Delta/kT)]\ .$$

$\Delta$ is the splitting of $d_{xz}$, $d_{yz}$ orbitals due to spin-orbit coupling $\xi_{3d}$ and rhombic distortion $\delta$ [32] (Fig. 8 and Table III) ; the eigenfunctions corresponding to the

Table III. — *Matrix elements of the perturbation* $\mathcal{H}_{\text{rhombic}} + \xi_{3d}\,\mathbf{l}.\mathbf{s}$ *in the basis of* $d_{xz}$ *and* $d_{yz}$ *wave functions.*

| | $\lvert d_{xz}\ 1/2\rangle$ | $\lvert d_{yz}\ 1/2\rangle$ | $\lvert d_{xz}\ -1/2\rangle$ | $\lvert d_{yz}\ -1/2\rangle$ |
|---|---|---|---|---|
| $\langle d_{xz}\ 1/2 \rvert$ | $-\frac{\delta}{2}$ | $0.83\, i\, \frac{\xi_{3d}}{2}$ | 0 | 0 |
| $\langle d_{yz}\ 1/2 \rvert$ | $-0.83\, i\, \frac{\xi_{3d}}{2}$ | $\delta/2$ | 0 | 0 |
| $\langle d_{xz}\ -1/2 \rvert$ | 0 | 0 | $-\delta/2$ | $-0.83\, i\, \frac{\xi_{3d}}{2}$ |
| $\langle d_{yz}\ -1/2 \rvert$ | 0 | 0 | $0.83\, i\, \frac{\xi_{3d}}{2}$ | $\delta/2$ |

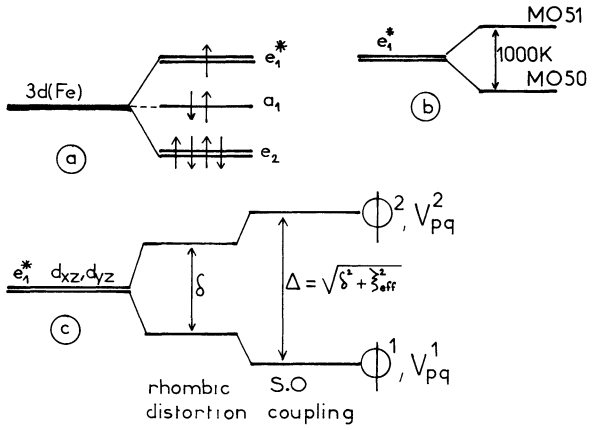


Fig. 8. — Molecular orbital energy levels : (*a*) $e_1^*$ in the axial ligand field is twice degenerated; (*b*) the effect of molecule distortion, 1 000 K is the energy difference between MO 50 and MO 51 according to MO calculations; (*c*) use of Ammeter's [16] model : the energy difference between $\phi_1$ and $\phi_2$ is due to the rhombic distortion and to the spin-orbit coupling. $V^1_{pq}$ and $V^2_{pq}$ are the EFG tensors corresponding to $\phi^1$ and $\phi^2$.

levels 1 and 2 of figure 8 are :

$$\phi^1 = \cos\theta\, d_{xz} + i \sin\theta\, d_{yz}$$

$$\phi^2 = -i \sin\theta\, d_{xz} + \cos\theta\, d_{yz}$$

with

$$\tan 2\theta = 0.83\, q\, \frac{\xi}{\delta} = \frac{\xi_{\text{eff}}}{\delta}.$$

This model is now used to analyse the thermal variation of the quadrupole splitting.

At high temperature, the EFG tensor remains constant from 190 K to 300 K. This implies that the orbital degeneracy of $e_1^*$ is not lifted (Fig. 8). The spin orbit coupling lifts the degeneracy but does not change the EFG tensor because it does not mix together the standard functions $\lvert 1\rangle$ and $\lvert -1\rangle$. The model gives $\Delta E_Q = 1.92 - 1.54 = 0.38$ mm/s to be compared with the experimental 0.5 mm/s. This 0.38 mm/s can be increased thanks to dynamic Jahn-Teller [18, 32] reduction of $V^{3d}_{pq}(T)$ by a factor $q = 0.9$. However inaccuracies of about 0.1 mm/s in this model do not allow any definite conclusions concerning this reduction.

At low temperature, the orbital degeneracy of $e_1^*$ is lifted according to the experimental change of the EFG tensor. The experimental $\Delta E_Q = -1.5$ mm/s can be fully explained by assuming thermal population of levels labelled 1 and 2 of figure 8*c*. According to the model, $\Delta E_Q = -1.5$ mm/s can be obtained for a rhombic distortion $\delta = 300$ K (leading to $\Delta = 535$ K) and $q = 0.9$.

**6. Conclusion.** — Experimental and calculated results concerning the electrostatic hyperfine interactions are in rather good agreement. This supports the reliability of the model based on MO calculations. A magnetic investigation of the paramagnetic complexes by Mössbauer spectroscopy will be further analysed.

## References


[1] COLLINS, R. L., *J. Chem. Phys.* **42** (1965) 1072.

[2] GREENWOOD, N. N., GIBB, T. C., *Mössbauer Spectroscopy* (Chapman and Hall) 1972, p. 222-238.

[3] STUKAN, R. A., VOL'KENAU, N. A., NESMEYANOV, A. N., GOLDANS'KII, V. I., *Izv. Akad. Nauk SSSR, Ser. Khim.* **8** (1966) 1472.

[4] TRAUTWEIN, A., RESCHKE, P., DEZSI, I., HARRIS, F. E., *J. Physique Colloq.* **37** (1976) C6-463.

[5] GREEN, M. L. H., *Organometallic compounds,* Vol. II, 1965.

[6] ASTRUC, D., HAMON, J. R., ALTHOFF, G., ROMAN, E., BATAIL, P., MICHAUD, P., MARIOT, J. P., VARRET, F., COZAK, D., *J. Am. Chem. Soc.* **101** (1979) 5445.

[7] HAMON, J. R., ASTRUC, D., MICHAUD, P., *J. Am. Chem. Soc.* **103** (1981) 758.

[8] *Image de la Chimie*, ed. CNRS, 1982, p. 10-13.

[9] GREEN, J. C., KELLY, M. R., PAYNE, M. P., SEDDON, E. A., ASTRUC, D., HAMON, J. R., MICHAUD, P., submitted to *Organometallics.*

[10] ASTRUC, D., ROMAN, E., HAMON, J. R., BATAIL, P., *J. Am. Chem. Soc.* **101** (1979) 2240.

[11] HAMON, J. R., ASTRUC, D., ROMAN, E., BATAIL, P., MAYERLE, J. J., *J. Am. Chem. Soc.* **103** (1981) 2431.

[12] ASTRUC, D., HAMON, J. R., ROMAN, E., MICHAUD, P., *J. Am. Chem. Soc.* **103** (1981) 7502.

[13] MICHAUD, P., ASTRUC, D., AMMETER, J. H., *J. Am. Chem. Soc.* **104** (1982) 3755.

[14] MICHAUD, P., ASTRUC, D., *J. C. S. Angew Chem.* **94** (1982) 921 ; *Angew. Chem. Int. Ed. Engl.* **21** (1982) 918.

[15] *a*) ANDERSON, S. E., DRACO, R. S., *J. Am. Chem. Soc.* **91** (1969) 3656 ;
*b*) *Ibid* **92** (1970) 4244 ;
*c*) RETTIG, M. F., DRAGO, R. S., *J. Am. Chem. Soc.* **91** (1969) 1361.

[16] AMMETER, J. H., *J. Magn. Reson.* **30** (1978) 299.

[17] For preliminary communication, see :
*a*) MARIOT, J. P., VARRET, F., MICHAUD, P., ASTRUC, D., HAMON, J. R., ALTHOFF, G., BATAIL, P., *J. Physique Colloq.* **41** (1980) C1-319.
*b*) MARIOT, J. P., MICHAUD, P., VARRET, F., ASTRUC, D., *Mössbauer Discussion Group of the Chemical Society,* London 1978 and Canterbury 1979.

[18] RAJASEKHARAN, M. V., GIESYNSKI, S., AMMETER, J. H., OSWALD, N., MICHAUD, P., HAMON, J. R., ASTRUC, D., *J. Am. Chem. Soc.* **104** (1982) 2400.

[19] X-ray structure data were taken from references 6 and 10.

[20] BATAIL, P., unpublished results.

[21] TRAUTWEIN, A., HARRIS, F. E., *Theor. Chim. Acta* **30** (1973) 45.

[22] CRODZICKI, M., LAUER, S., TRAUTWEIN, A., VERA, A., in « Recent Chemical Applications of Mössbauer Spectroscopy », eds. J. Stevens and G. Shenov, *Adv. Chem. Ser.* **194** (ACS, Washington D.C.) 1981.

[23] TRAUTWEIN, A., HARRIS, F. E., FREEMAN, A. T., DESCLAUX, J. P., *Phys. Rev.* B **11** (1975) 4101.

[24] CLEMENTI, E., ROETTI, C., *At. Data Nucl. Data Tables* **14** (1974) 177.

[25] LEROCHEREUIL, P., DEA, Le Mans 1981.

[26] VARRET, F., *J. Phys. Chem. Solids* **37** (1976) 265.

[27] STERNHEIMER, R. M., *Phys. Rev.* **146** (1966) 140.

[28] SEN, K. D., NARASIMHAN, P. T., *Phys. Rev. B* **16** (1977) 107.

[29] LAUER, S., MARATHE, V. R., TRAUTWEIN, A., *Phys. Rev. A* **19** (1979) 1852.

[30] STERNHEIMER, R. M., *Phys. Rev.* **95** (1954) 736.

[31] *Topics in Applied physics*, ed. U. Gonser, p. 57 (Springer Verlag) 1975.

[32] AMMETER, J. H., SWALEN, J. D., *J. Chem. Phys.* **57** (1972) 678.

[33] COLLINS, R. L. and TRAVIS, J. C., *Mössbauer effect methodology* (1967) vol. 3 (I. J. Gruvernam, ed.).

[34] TEILLET, J., VARRET, F., unpublished MOSHEX program.